Plant Biotechnology Journal
Open Access

Plant Biotechnology Journal (2023) **21**, pp. 621–634 doi: 10.1111/pbi.13976

MATE transporter GFD1 cooperates with sugar transporters, mediates carbohydrate partitioning and controls grain-filling duration, grain size and number in rice

Changhui Sun[1,*,†], Yang Wang[1,2,†], Xiaorong Yang[1,†], Lu Tang[3,†], Chunmei Wan[1,†], Jiqing Liu[1,†], Congping Chen[1], Hongshan Zhang[1], Changcai He[1], Chuanqiang Liu[1], Qian Wang[1], Kuan Zhang[1], Wenfeng Zhang[1,2], Bin Yang[1], Shuangcheng Li[1], Jun Zhu[1], Yongjian Sun[1], Weitao Li[1], Yihua Zhou[2], Pingrong Wang[1,*] and Xiaojian Deng[1,*]

[1]*State Key Laboratory of Crop Gene Exploration and Utilization in Southwest China, Rice Research Institute, Sichuan Agricultural University, Chengdu, China*
[2]*College of Agricultural Science, Panxi Crops Research and Utilization Key Laboratory of Sichuan Province, Xichang University, Liangshan, China*
[3]*State Key Laboratory of Plant Genomics, Institute of Genetics and Developmental Biology, The Innovative Academy for Seed Design, Chinese Academy of Sciences, Beijing, China*

Received 8 April 2022;
revised 13 November 2022;
accepted 4 December 2022.
**Correspondence* (Tel +86 28 86290903; fax +86 28 82652669; email sunhui0307@163.com (CS), Tel +86 28 86290903; fax +86 28 82652669; email prwang@sicau.edu.cn (PW), Tel +86 28 86290903; fax +86 28 82652669; email xjdeng@sicau.edu.cn (XD))
[†]These authors contributed equally to this work.

Keywords: carbohydrate partitioning, grain-filling duration, MATE transporter, sugar transporter, rice.

Summary

More than half of the world's food is provided by cereals, as humans obtain >60% of daily calories from grains. Producing more carbohydrates is always the final target of crop cultivation. The carbohydrate partitioning pathway directly affects grain yield, but the molecular mechanisms and biological functions are poorly understood, including rice (*Oryza sativa* L.), one of the most important food sources. Here, we reported a prolonged *grain filling duration mutant 1* (*gfd1*), exhibiting a long grain-filling duration, less grain number per panicle and bigger grain size without changing grain weight. Map-based cloning and molecular biological analyses revealed that *GFD1* encoded a MATE transporter and expressed high in vascular tissues of the stem, spikelet hulls and rachilla, but low in the leaf, controlling carbohydrate partitioning in the stem and grain but not in the leaf. GFD1 protein was partially localized on the plasma membrane and in the Golgi apparatus, and was finally verified to interact with two sugar transporters, OsSWEET4 and OsSUT2. Genetic analyses showed that GFD1 might control grain-filling duration through OsSWEET4, adjust grain size with OsSUT2 and synergistically modulate grain number per panicle with both OsSUT2 and OsSWEET4. Together, our work proved that the three transporters, which are all initially classified in the major facilitator superfamily family, could control starch storage in both the primary sink (grain) and temporary sink (stem), and affect carbohydrate partitioning in the whole plant through physical interaction, giving a new vision of sugar transporter interactome and providing a tool for rice yield improvement.

Introduction

All living organisms require organic carbon to grow and survive. Many eukaryotes, including humans, cannot produce carbon supply by themself. More than half of the world's food is provided by cereals, as humans obtain >60% of daily calories from grains (Alexandratos and Bruinsma, 2012; Julius *et al.*, 2017). Assimilating, transporting and distributing carbohydrates from leaves to sink tissues are fundamental to cereals' yield (Durand *et al.*, 2018; Julius *et al.*, 2017; Zhang and Turgeon, 2018). Consequently, understanding carbohydrate partitioning and its genetic regulation mechanism could lead to a breakthrough in crop yield, including rice (*Oryza sativa* L.), one of the most important food sources (Wei *et al.*, 2017).

Sucrose, the primary carbohydrate form, is produced by photosynthetic source tissues such as leaf blades and transported to other tissues via a continuous mature phloem transport system. This system comprises phloem sieve elements connected end to end, combining the whole plant organs. Generally, sucrose is firstly loaded into the phloem in source tissues, then transported via the long-distance vascular channels and finally unloaded into sink tissues (Julius *et al.*, 2017; Scofield *et al.*, 2007b; Zhang *et al.*, 2007). The primary sink tissue is grain, where the sucrose is mainly stored as starch. In the grain-filling process, sucrose flows directly along the pedicel's central vasculature distributing in the whole panicle, then through the rachilla and pericarp dorsal vascular bundle and finally into the endosperm for starch synthesis (Scofield *et al.*, 2007b; Zee, 1972). Besides, temporary starch granules (SGs) stored in the stem can be acted as a temporary sink. These SGs can convert to sucrose again, return to the long-distance pathway and be transported into the panicle's filling grain. Up to 24–27% of the carbohydrate in the grain originates from stem starch reserves (CocK and Yoshida, 1972). However, the sugar transportation mechanism remains unclear in rice.

In most monocots, the long-distance transport of sucrose may be involved in the apoplastic pathway that requires sugar transporters SUT (sucrose transporter) and Sugars Will Eventually be Exported Transporters (SWEET) to facilitate sugars movement between cells (Eom *et al*., 2011; Julius *et al*., 2017). SUTs load sucrose against its prevailing concentration gradients into the phloem. By comparison, SWEETs appear to function as facilitators that promote transport down the sucrose gradients (Mathan *et al*., 2021b; Wu *et al*., 2018). In the genome of rice, there are five SUT genes. *OsSUT1*, *OsSUT3*, *OsSUT4* and *OsSUT5* encode plasma membrane-localized proteins, and OsSUT2 is localized on the tonoplast membrane (Aoki *et al*., 2003; Eom *et al*., 2011; Siao *et al*., 2011). *OsSUT1* is expressed after heading in the filling grain, leaf sheath, stem, nucellus, vascular parenchyma tissue and the nucellar projection (Matsukura *et al*., 2000; Scofield *et al*., 2007b). *OsSUT1* might take part in sugar assimilation along the long-distance pathway, from the leaf to the base of the filling grain (Furbank *et al*., 2001; Hirose *et al*., 2010; Matsukura *et al*., 2000; Scofield *et al*., 2007b). *OsSUT2* is highly expressed in leaf mesophyll cells, emerging lateral roots, pedicels of fertilized spikelets and cross-cell layers of grain coats (Aoki *et al*., 2003; Eom *et al*., 2011). The *ossut2* mutant exhibits a growth retardation phenotype of tiller number, plant height, 1000-grain weight and so on (Eom *et al*., 2011). *OsSUT2* is most likely involved in sucrose transport across the tonoplast from the vacuole to the cytosol (Eom *et al*., 2011; Siao *et al*., 2011). *OsSUT3* transcripts likely accumulate in sink leaves and exposed internode-1, but not in the enclosed region (Aoki *et al*., 2003; Scofield *et al*., 2007b). *OsSUT4* shows preferential expression in sink leaves and stems (Aoki *et al*., 2003; Scofield *et al*., 2007b). *OsSUT5* is expressed most in sink leaves (Aoki *et al*., 2003; Scofield *et al*., 2007b; Sun *et al*., 2010). Among 21 *OsSWEET* genes in rice, *OsSWEET4* and *OsSWEET11* have major effects on caryopsis development (Li *et al*., 2022), and *ossweet4* is even defective in grain filling (Sosso *et al*., 2015). The double-knockout mutant *ossweet11 ossweet15* exhibits unfunctional endosperm and no accumulated starch in the grain (Ma *et al*., 2017; Yang *et al*., 2018). However, we still know little about how these sugar transporters work until now.

Multidrug and toxic compound extrusion transporters (MATEs) are a category of cation antiporters in most organisms and constitute one of the largest transporter families (Omote *et al*., 2006; Takanashi *et al*., 2014). MATE transporters are involved in various physiological functions in the plant, transporting a broad range of substrates such as organic acids, plant hormones and secondary metabolites (Takanashi *et al*., 2014; Wang *et al*., 2016). Members of this family mediate the export of organic substrates with the coupled exchange of Na^+ or H^+, and are driven by the electrochemical gradient across the membrane (Kuroda and Tsuchiya, 2009; Omote *et al*., 2006). There are at least 50 MATE family members in rice (Yokosho *et al*., 2016), but none has been reported to take part in sugar transportation.

Here, we reported a prolonged *grain filling duration mutant 1* (*gfd1*) exhibiting a long grain-filling duration, less grain number per panicle and bigger grain size without changing grain weight. Map-based cloning and molecular biological analyses revealed that *GFD1* encoded a MATE transporter and expressed high in vascular tissues of the stem, spikelet hulls and rachilla, but low in the leaf, controlling carbohydrate partitioning in the stem and grain but not in the leaf. GFD1 proteins are partially localized on the plasma membrane and in the Golgi apparatus and interact with two sugar transporters, OsSWEET4 and OsSUT2. Genetic analyses further showed that GFD1 might control grain-filling duration through OsSWEET4, regulate grain size together with OsSUT2 and synergistically modulate grain numbers per panicle with OsSUT2 and OsSWEET4. Together, our study characterized GFD1 as an important regulator in carbohydrate partitioning and revealed a molecular mechanism involving grain-filling duration, grain size and number per panicle, which may provide a tool for rice yield improvement.

Results

Prolonged grain-filling duration mutant *gfd1* shows pleiotropic phenotypes

By screening the mutant library derived from the chemical mutagenesis of G46B (an *indica* variety), we identified a prolonged grain-filling duration mutant *gfd1* (Figure 1a). Though the heading date of *gfd1* (74 days) was about 4 days later than G46B (70 days), the mature period of *gfd1* was more than 15 days longer than G46B. To eliminate the differences in the mature period due to later heading, we examined the grain weight every 3 days from the first day after fertilization (DAF) to the mature stage in *gfd1* and G46B. The results showed that the period from fertilization to the largest grain weight day was more than 10 days longer in *gfd1* than in the wild type (WT) (Figure 1g,h). The reduced grain weight of *gfd1* in the early ripening stage indicated its grain-filling rate was slowed down (Figure 1g,h). However, the mature grain weight of *gfd1* (45 DAF) was comparable with that of the WT due to a longer grain-filling duration (Figure 1h).

Grain filling is highly correlated with grain quality. We thus compared the grain appearance between the mutant and WT. The unshell mature *gfd1* grains and the cross-sections appeared brown-pink and opaque, whereas those of WT looked translucent with partial chalk (Figure 1d). Scanning electron microscopy of the endosperms further exhibited that the SGs in *gfd1* endosperm were loosely packed, resulting in large sizes of SGs with irregular shapes; those in the WT were quite small and tightly organized (Figure 1d). Chemical examination revealed that *gfd1* grains contained higher sucrose, glucose and fructose, but lower starch proportions than the WT (Figure 1i–l). Furthermore, *gfd1* displayed additional abnormal agronomic traits, such as bigger grain, less grain number per panicle and a reduced yield (Figures 1b,c,e,f, S1). Therefore, *GFD1* mutation compromises grain starch synthesis in the grain-filling process and negatively regulates plant yield.

Map-based cloning of *GFD1*

For genetic analysis, an F_2 population was constructed by crossing the mutant *gfd1* with its WT variety G46B. In this population, the longer grain-filling duration and normal grain-filling duration plants were segregated as 145:476 ($P > 0.05$), suggesting that a single Mendelian factor controlled the grain-filling duration of *gfd1* (Figure 2a). Moreover, the grain width and length, and the grain number per panicle were perfectly cosegregated with the grain-filling duration (Figure 2b–d). These results suggested that the pleiotropic variations of *gfd1* might be caused by the same locus.

We applied a map-based cloning method to identify the responsible gene *GFD1* (Figure 2). Sixty-five individuals with extremely slower grain filling were chosen from the F_2 population crossing by *gfd1* and ZH11. *GFD1* was first located in the short

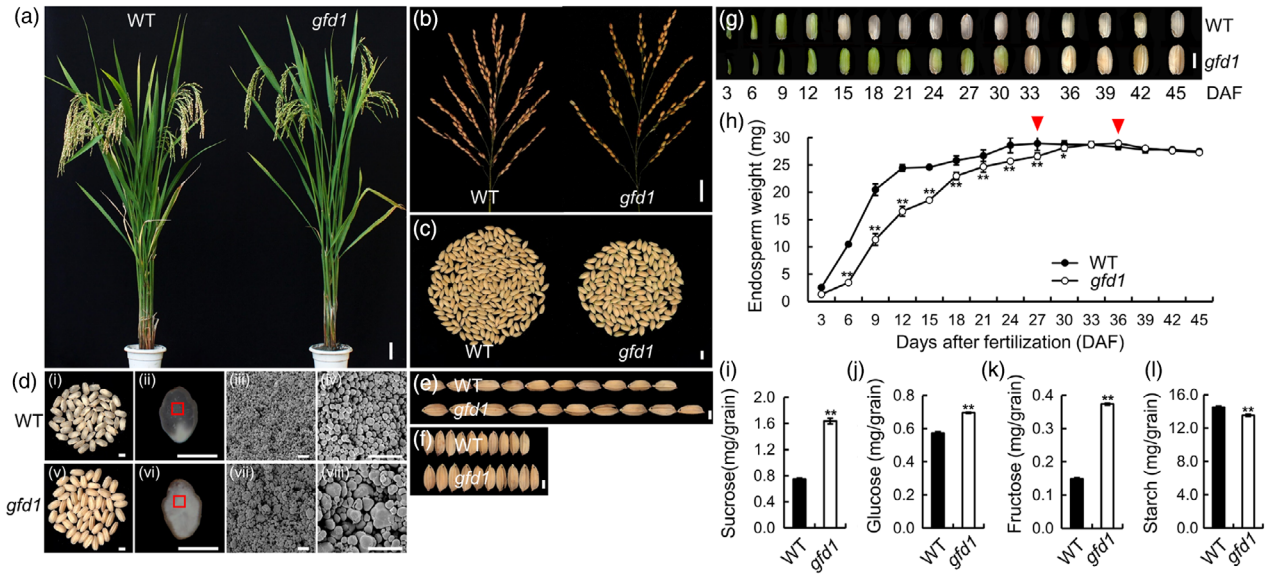

Figure 1 Phenotypes characterization of wild-type (WT) and *gfd1* mutant. (a) Plant architecture of WT and *gfd1* plants at the grain-filling stage. Scale bar, 10 cm. (b) Panicle architecture of WT and *gfd1* mutant. Scale bar, 3 cm. (c) Decreased grain number per panicle in *gfd1*. Scale bar, 5 mm. (d) Caryopsis characterization of WT and *gfd1*. (i, v) Appearance comparison of caryopsis. (ii, vi) Transverse sections of caryopsis. (iii, iv, vii, viii) Scanning electron microscopy analysis of transverse sections of WT (iii, iv) and *gfd1* (vii, vii) endosperms. Scale bars, 3 mm (i–ii, v–vi); 20 μm (iii–iv, vii–vii). (e, f) Comparison of grain length (e) and grain width (f) in WT and *gfd1*. Scale bars, 3 mm. (g) Fresh caryopsis of WT and *gfd1* at various development stages. DAF, days after fertilization. Scale bar, 3 mm. (h) Weight statistics of fresh caryopsis. The maximum weight values of WT and *gfd1* were indicated with red triangles, respectively. (i–l) Sucrose, glucose, fructose and starch content of WT and *gfd1* grains. Data in (h, –l) are shown as means ± SD from three biological replicates. Asterisks indicate statistically significant differences by a Student's *t*-test (**P* < 0.05; ***P* < 0.01).

arm of chromosome 3 between the simple sequence repeat (SSR) marker RM218 and InDel marker C1 (Figure 2e). Then, 1 SSR and 9 InDel markers possessing polymorphisms between the two parents were developed (Table S1). Using 232 slower grain-filling individuals in the B_2F_2 population (*gfd1* × ZH11), we further narrowed down the locus of *GFD1* to a 121 kb region between RM3716 and C7 (Figure 2f).

For hyperfine mapping, we constructed a B_4F_2 generation population (*gfd1* × ZH11) and designed 3 single-nucleotide polymorphism (SNP) markers. Thousand eight hundred sixty individuals with a slower grain-filling phenotype were carefully selected. The localization interval was finally narrowed to 7.3 kb between S1 and C6 markers, containing only one open reading frame *LOC_Os03g12790* (Figure 2g,h). *LOC_Os03g12790* encodes a MATE transporter, one of the largest transporter families in the plant (Takanashi *et al*., 2014; Wang *et al*., 2016). Full-length amplification and sequencing of the genome and cDNA of *LOC_Os03g12790* showed that *gfd1* had a single base mutation (G to A) in the second exon, which changed the amino acid Glu to Lys in the MATE1 domain (Figure 2h).

Complementation and CRISPR/Cas9 knockout of *GFD1*

The full-length 6.2 kb genome fragment of *LOC_Os03g12790* containing its promoter was jointed to the pCAMBIA1300 vector for the complementation test. Because the *indica* variety G46B is recalcitrant to transform, we introduced the complementation constructor into the near-isogenic line of *gfd1* in the ZH11 background (NIL^{ZH11}). We obtained 20 independent-positive T_0 lines holding a normal grain-filling duration as the WT (Figure 3). In T_1 generation lines, normal and slower grain-filling individuals were *segregated*, and the positive individuals were all co*segregated with the normal grain filling phenotype*. Besides, other agronomic trait variations in NIL^{ZH11}, such as larger grain size and less grain number per panicle, were also restored to the WT level (Figures 3, S2).

Further validation was achieved by knockout *GFD1* in ZH11 (KO1 and KO2) and Nipponbare (KO3) using the CRISPR/Cas9 system. Two sgRNA targeting sequence sites on the second exon of *GFD1* for CRISPR/Cas9 cleavage were applied, respectively (Figure S3). We obtained more than eight independent knockout lines in the two backgrounds. All the knockout lines showed similar phenotypic mutations of *gfd1*, longer grain-filling duration, bigger grain size and less grain number per panicle (Figures 3, S4–S8). Taken together, *LOC_Os03g12790* was considered to be the responsible gene for the mutation of *gfd1*.

Expression pattern and subcellular localization

Temporal and spatial expression analysis by quantitative RT-PCR (qRT-PCR) showed that *GFD1* was constitutively expressed in all tested organs (Figure 4a). However, the transcript levels were higher in the booting stem, heading stem, heading leaf sheath and panicle but lower in leaves. The stem at the heading stage possessed the highest transcription level, indicating the importance of *GFD1* in the stem of this stage.

Moreover, a vector with a GUS reporter gene driven by the *GFD1* promoter was constructed and transformed into ZH11. Histochemical analysis revealed that strong GUS signals were detected in the stem, spikelet hull and rachilla (Figure 4b). Consistent with the qRT-PCR results, there were weak GUS signals in the leaf, suggesting a feeble function of *GFD1* in the leaf. During the grain filling and mature process, GUS signals were dynamically changed in the caryopsis: gradually increased

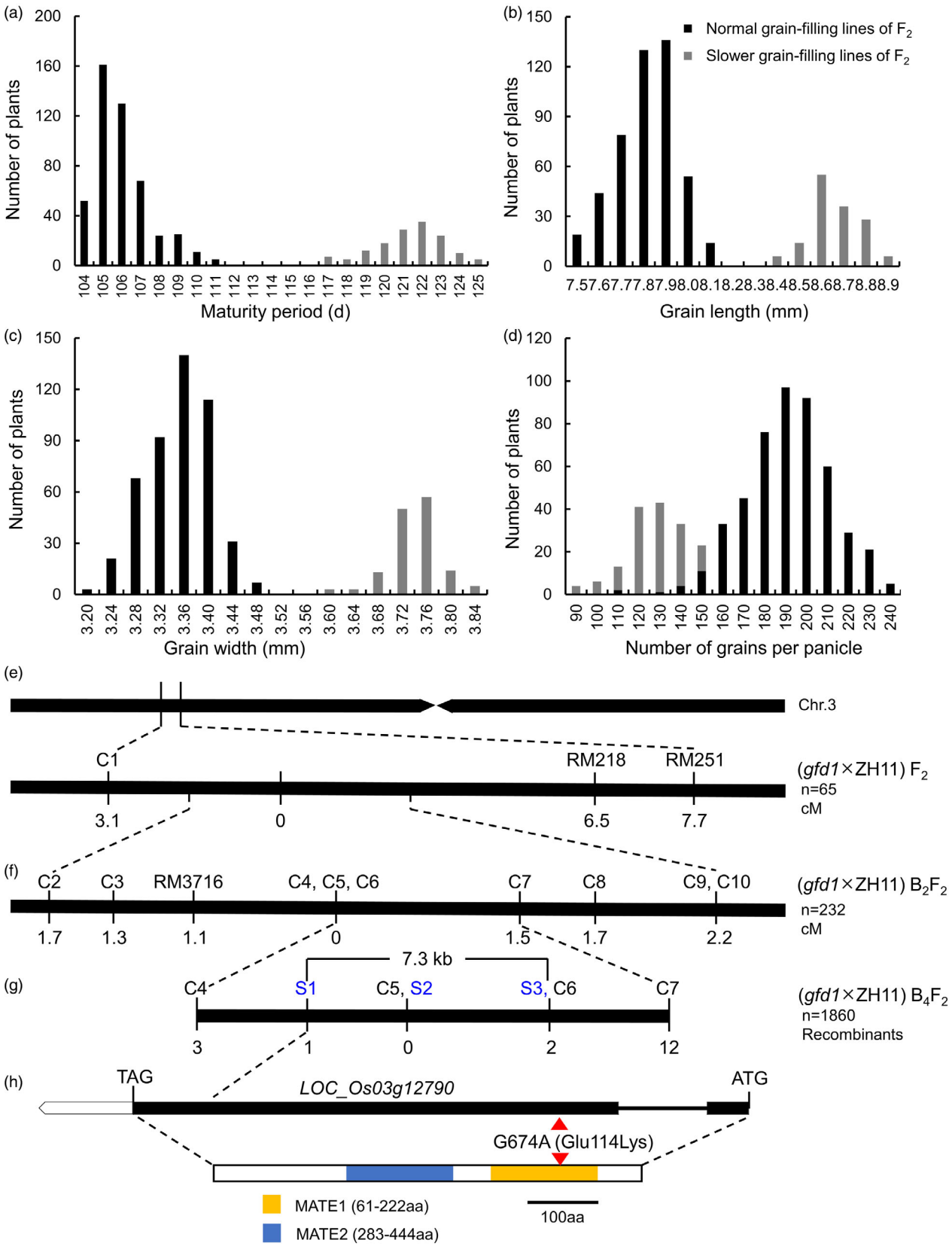
(a)
Number of plants
Maturity period (d)
(b)
Normal grain-filling lines of F2
Slower grain-filling lines of F2
Number of plants
Grain length (mm)
(c)
Number of plants
Grain width (mm)
(d)
Number of plants
Number of grains per panicle
(e)
Chr.3
C1
RM218
RM251
(gfd1×ZH11) F2
n=65
cM
(f)
C2
C3
RM3716
C4, C5, C6
C7
C8
C9, C10
(gfd1×ZH11) B2F2
n=232
cM
(g)
7.3 kb
C4
S1
C5, S2
S3, C6
C7
(gfd1×ZH11) B4F2
n=1860
Recombinants
(h)
TAG
LOC_Os03g12790
ATG
G674A (Glu114Lys)
MATE1 (61-222aa)
MATE2 (283-444aa)
100aa

Figure 2 Map-based cloning of *gfd1*. (a–d) Distribution statistics of plant numbers in maturity period (a), grain length (b), grain width (c) and the number of grains per panicle (d) in F_2 populations (G46B × *gfd1*). Maturity period was determined by heading date and grain-filling duration. In *gfd1*, there was no significant change in the heading date, and the maturity period was mainly dependent on grain-filling duration. (e) *GFD1* was primarily mapped to the short arm of chromosome 3 between InDel marker C1 and simple sequence repeat (SSR) marker RM251. (f) The interval was narrowed to 121 kb between RM3716 and C7. (g) Delimitate *GFD1* to a 7.3-kb region between single-nucleotide polymorphism (SNP) marker S1 and InDel marker C6 using 1860 homozygous B_4F_2 plants. (h) Gene structure and mutation site of *GFD1*. The candidate gene *LOC_Os03g12790* comprises two exons and one intron, and its encoding protein contains two domains (MATE1 and MATE2). A single-nucleotide G-to-A substitution at 674 bp at the coding region in *gfd1* was indicated with the red triangles.

from 6 DAF to 12 DAF, maintained at a high level from 12 DAF to 21 DAF, then decreased from 21 DAF to 27 DAF and finally shrunk in the pericarp dorsal vascular bundle of the caryopsis which was also reconfirmed under a microscope (Figure 4b, vi and vii). *In situ* hybridization also showed that *GFD1* preferred to express in the pericarp and dorsal vascular bundle of caryopsis (Figure 4c, iv–vi). Besides, both GUS histochemical (Figure 4b, iii) and *in situ* hybridization (Figure 4c, i–iii) analyses showed that *GFD1* could express in sclerenchyma cell, parenchymal cell and vascular bundles in the stem. Consequently, *GFD1* was mainly expressed in the vital organization for substance transport in stem and grain.

Plant MATE transporters are located in different compartments, such as plasma membrane, vacuolar membrane and Golgi complex (Upadhyay *et al.*, 2019; Wang *et al.*, 2016). The GFD1 protein was predicted as a MATE transporter containing two domains (MATE1 and MATE2) with no apparent signal peptide (www.ncbi.nlm.nih.gov, www.cbs.dtu.dk). For subcellular localization detection, GFD1-GFP and GFP-GFD1 constructors driven by the CaMV35S promoter were transiently transformed into rice protoplasts. As shown in Figure 4d, GFP signals of both GFD1-GFP and GFP-GFD1 fusion proteins might partly distribute on the plasma membrane. Therefore, OsRAC3, a plasma membrane-localized protein, was used as a plasma membrane marker (Chen *et al.*, 2010). GFD1-GFP was co-transformed with OsRAC3-mRFP into rice protoplasts and *Nicotiana benthamiana* leaves. The results showed that the fluorescences of OsRAC3-mRFP and GFD1-GFP could be merged as white light in the plasma

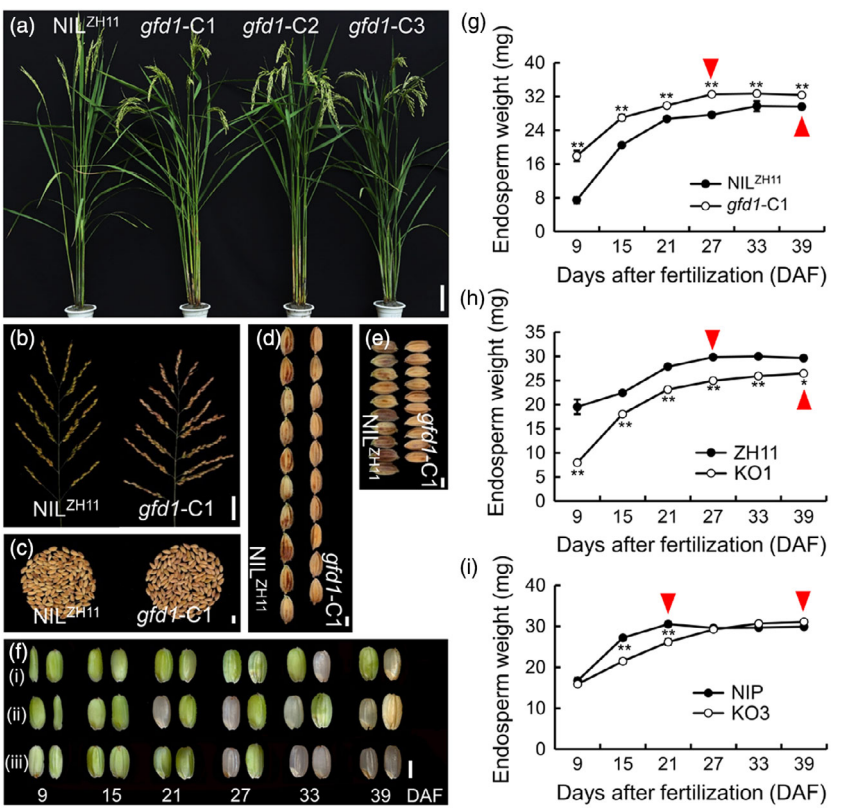

Figure 3 Function verification of *GFD1* by complementation and CRISPR/Cas9 knockout. (a) Plant architecture of the NIL^{ZH11} (NIL of *gfd1* in ZH11 background) and *gfd1*-C (complementary lines) at the grain-filling stage. *gfd1*-C1, *gfd1*-C2 and *gfd1*-C3 are three independent transgenic lines. Scale bar, 10 cm. (b) Panicle architecture of NIL^{ZH11} and *gfd1*-C1. Scale bar, 3 cm. (c) Comparing grain number per panicle between NIL^{ZH11} and *gfd1*-C1. Scale bar, 5 mm. (d, e) Comparison of grain length (e) and grain width (f) in NIL^{ZH11} and *gfd1*-C1. Scale bars, 3 mm. (f) Caryopsis comparison at 9, 15, 21, 27, 33 and 39 day after fertilization (DAF) in (i) the NIL^{ZH11} (left) and *gfd1*-C1 (right), (ii) ZH11 (left) and KO1 (right), and (iii) Nipponbare (left) and KO3 (right). Scale bars, 3 mm. (g–i) Caryopsis weight at various stages of grain filling in NIL and *gfd1*-C (h), ZH11 and KO1 (j), and Nipponbare and KO3 (i). The maximum weight is indicated with a red triangle in (h, i). Data in (h, i) are given as means ± SD from three biological replicates. Asterisks indicate statistically significant differences by a Student's *t*-test (*$P < 0.05$; **$P < 0.01$).

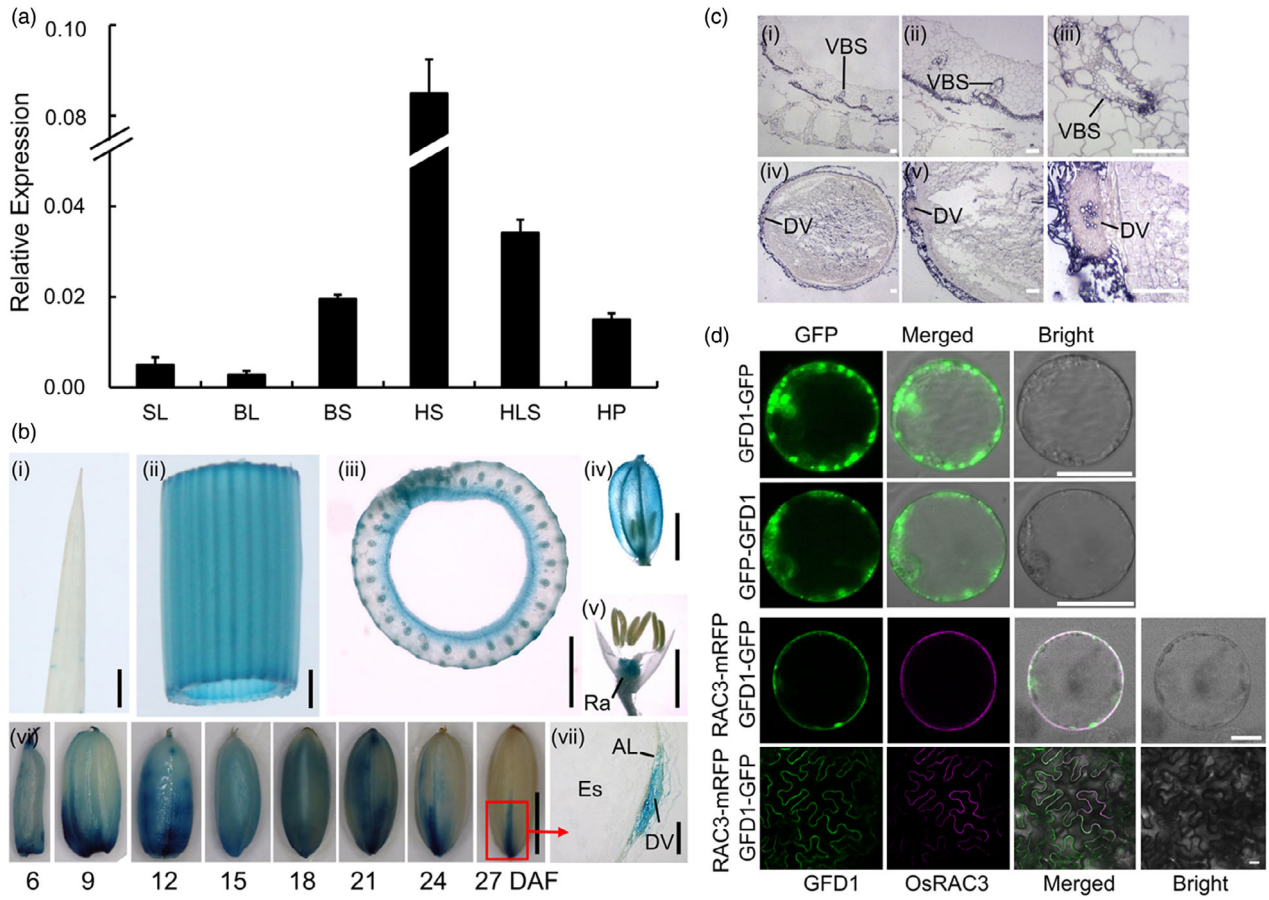

Figure 4 Expression pattern and subcellular localization. (a) *GFD1* transcript levels in various tissues detected by qRT-PCR. Rice *Actin1* was used as an internal control. SL, seedling leaf; BL, booting leaf; BS, booting stem; HS, heading stem; HLS, heading leaf sheath; HP, heading panicle. Data are given as means ± SD from three biological replicates. (b) GUS staining in leaf (i), stem (ii, iii), spikelet (iv, v) and developing caryopsis (vi) driven by *GFD1* promoter. (vii) Transverse section of caryopsis at 30 day after fertilization (DAF). Ra, rachilla; Es, endosperm; AL, aleurone layer; DV, dorsal vascular bundle. Scale bars, 5 mm (i); 3 mm (iv–vi); 1 mm (ii, iii); 100 μm (vii). (c) *GFD1* mRNA accumulation pattern detected by *in situ* hybridization in transverse sections of the stem at the booting stage (i–iii) and the caryopsis at 9 DAF (iv–vi) in G46B. VBS, vascular bundles; DV, dorsal vascular bundle. Scale bars, 100 μm. (d) Subcellular localization of GFD1. GFP was fused into C- or N- terminal of GFD1, respectively. OsRAC3-mRFP was used as a plasma membrane marker. The scale bars represent 10 μm in rice protoplast cells and 20 μm in tobacco leaves.

membrane (Figure 4d). Besides, uneven spot-like distribution of fluorescent signals of GFD1 was also observed in the cytoplasm in rice protoplasts and *N. benthamiana* leaves.

By analysing the spot-like signals' characteristics, GFD1 is not likely to localize in the nucleus, chloroplast and endoplasmic reticulum (Nelson *et al.*, 2007). As a result, the punctate signals of GFD1 are similar to the Golgi apparatus. Therefore, we co-transformed GFD1-GFP with Golgi marker Man49-mRFP or ERD2-mRFP, respectively (Li *et al.*, 2009a; Montesinos *et al.*, 2014). The results showed that the punctate signals of GFD1 could partially merge with Man49 or ERD2 as white light (Figure S9). However, some punctate signals are still out of the Golgi apparatus, suggesting the complex subcellular localization of GFD1. In summary, the GFD1 protein could partially localize on the plasma membrane and in the Golgi apparatus.

gfd1 disordered carbohydrate distribution in stem and grain but not leaf

In rice, the primary form of the assimilated carbon is sucrose, which is transported starting from the leaf (source), through long-distance transport in the stem (flow), and finally reaches the vascular trace of seed (sink) (Krishnan and Dayanandan, 2003; Sturm and Tang, 1999). And then, the sucrose is hydrolysed in the extracellular space into monosaccharides and transported into the endosperm by sugar transporters such as OsSWEET4 for starch synthesis (Wang *et al.*, 2008). Each of the steps above changes could affect the grain-filling results. Therefore, to probe the physiological basis of the *gfd1* mutant phenotype, we detected the carbohydrate distribution of *gfd1* in leaf, stem or grain under four development stages, including the heading stage before pollination, 9 DAF, 15 DAF and after the grain-filling stage (Figure 5).

In the immature grain of *gfd1*, the starch content was significantly decreased in the 9 and 15 DAF (Figure 5a). However, sucrose, glucose and fructose were increased (Figure 5b–d). It was consistent with the results in the mature grain of *gfd1* (Figure 1i–l). More sugar but less starch in the immature and mature grain of *gfd1* suggested that *GFD1* could participate in some steps of sugar transport and thus affect the starch synthesis rate in the grain.

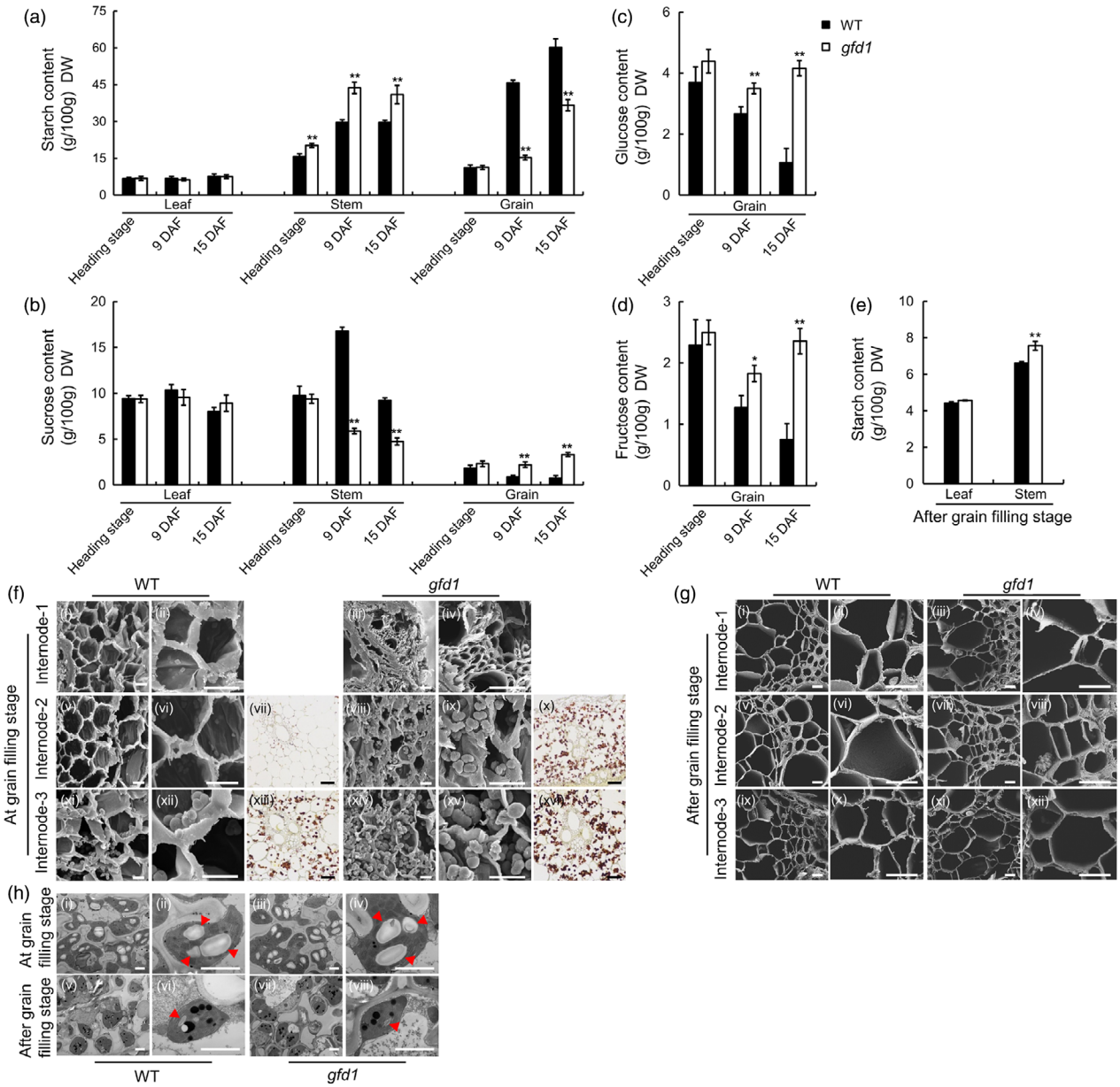

Figure 5 Carbohydrate partitioning was disordered in *gfd1*. (a, b) Starch and sucrose content in leaf, stem and grain at the heading stage, 9 day after fertilization (DAF) and 15 DAF. (c, d) Glucose and fructose content in grain at the heading stage, 9 DAF and 15 DAF. (e) Starch content in leaf and stem after the grain-filling stage. At the grain-filling stage is about 5 days after heading. After, the grain-filling stage is about 47 days after heading and with mature grain. Data in (a–e) are given as means ± SD at least three independent assays. DW means dry weight. Asterisks indicate statistically significant differences by Student's *t*-test (*$P < 0.05$; **$P < 0.01$). (f) Starch granules (SGs) were detected in the stem of WT and *gfd1* at the grain-filling stage. Scanning electron microscopy images showed the cross-sections of internode-1 (i, ii, iii, iv), internode-2 (v, vi, viii, ix), internode-3 (xi, xii, xiv, xv). Starch iodine staining images showed the cross-sections of internode-2 (vii, x) and internode-3 (xiii, xvi). Scale bars, 20 μm. (g) SGs were detected in the stem of WT and *gfd1* after the grain-filling stage. Scanning electron microscopy images showed the cross-sections of internode-1 (i, ii, iii, iv), internode-2 (v, vi, vii, viii) and internode-3 (ix, x, xi, xii). Scale bars, 5 μm. (h) Ultrastructure of chloroplasts in mesophyll cells at and after the grain-filling stages. There was no significant difference in SG accumulation in the chloroplasts between WT and *gfd1*. Both WT and *gfd1* exhibited more SG accumulation at the grain-filling stage and less SG accumulation after the grain-filling stage. Red arrows indicate SGs. Scale bars, 2 μm.

In the *gfd1* stem, the sucrose flow was sharply decreased after pollination (Figure 5b), along with a significant starch accumulation, especially in 9 and 15 DAF (Figure 5a). As described previously, starch accumulation tended to be higher in the basal but lower in the apical internodes in rice (Bihmidine *et al.*, 2015; Julius *et al.*, 2017). Scanning electron microscope data demonstrated that this conclusion still worked in our study. At the grain-filling stage (about 5 days after heading), internode-2 and internode-3 but not internode-1 displayed a higher SGs density in *gfd1*, which was further confirmed by iodine-stained (Figure 5f). As a result, sucrose in *gfd1* stem is more likely to convert into starch instead of being transported to grain at the

grain-filling stage. However, such SG accumulation was significantly reduced in WT and *gfd1* after the grain-filling stage (about 47 days after heading, Figure 5g), which was reconfirmed by the starch content measurement (Figure 5e), implying that most of the SGs in the stem had been transported into seeds after complete filling.

Interestingly, the carbohydrate distribution in the leaf was not the same as that in the stem, since the starch or sucrose contents were unchanged under the four development stages in *gfd1* (Figure 5a,b,e). In the leaf, starch accumulation usually occurs in the chloroplast. Thus, we detected the accumulation of SGs in the chloroplast of the leaf in WT and *gfd1* by transmission electron microscopy. Consistent with the measurement results of starch content in the leaves (Figure 5a,e), there was no significant difference in SG accumulation between WT and *gfd1* at or after the grain-filling stage (Figure 5h). Accordingly, *GFD1* mediates sugar transport in both stem and grain but not in the leaf in rice.

GFD1 affects the expression of starch synthesis and sugar transporter genes

For transcriptional basis exploration of *gfd1*, starch synthesis genes (*OsAGPL2*, *OsBE1*, *OsBEIIb*, *OsSSI*, *OsSSIIa*, *OsSSIIIa* and *OsGBSSI*) and sugar transporters (*OsSUTs* and *OsSWEETs*) were selected and detected in the booting stem, and 3 DAF stem and grain (Durand *et al.*, 2018; Li *et al.*, 2017). The qRT-PCR results showed that lesions in *GFD1* altered the expression balance of starch synthesis and sugar transport genes. In *gfd1*, most sugar transporters' expression levels were down-regulated in the stem (Figure 6b), but increased in the grain 3 DAF (Figure 6d). Meanwhile, consisting of the higher starch content in the stem and lower starch synthesis rate in the grain in *gfd1*, all the starch synthesis genes were up-regulated in the stem (Figure 6a), while most of them were down-regulated in the grain (Figure 6c).

GFD1 interacts with OsSUT2 and OsSWEET4 *in vitro* and *in vivo*

GFD1 affects carbohydrate distribution, and its expression pattern and subcellular localization are similar to some sugar transporters (Chen *et al.*, 2012; Hirose *et al.*, 2010; Matsukura *et al.*, 2000; Scofield *et al.*, 2007a,2007b). Thus, we wanted to determine whether GFD1 could interact with sugar transporters for sugar transportation. Then, we designed several experiments. Firstly, we screened the candidate sugar transporters in OsSUTs and OsSWEETs by yeast two-hybrid assays. The results revealed that the MATE1 but not MATE2 domain of GFD1 could interact with OsSUT2 and OsSWEET4 in yeast (Figures 7a, S10, S11). Moreover, we also amplified the mutant MATE1^{gfd1} fragment from *gfd1*, inserted it into the AD vector and co-transformed it with OsSUT2

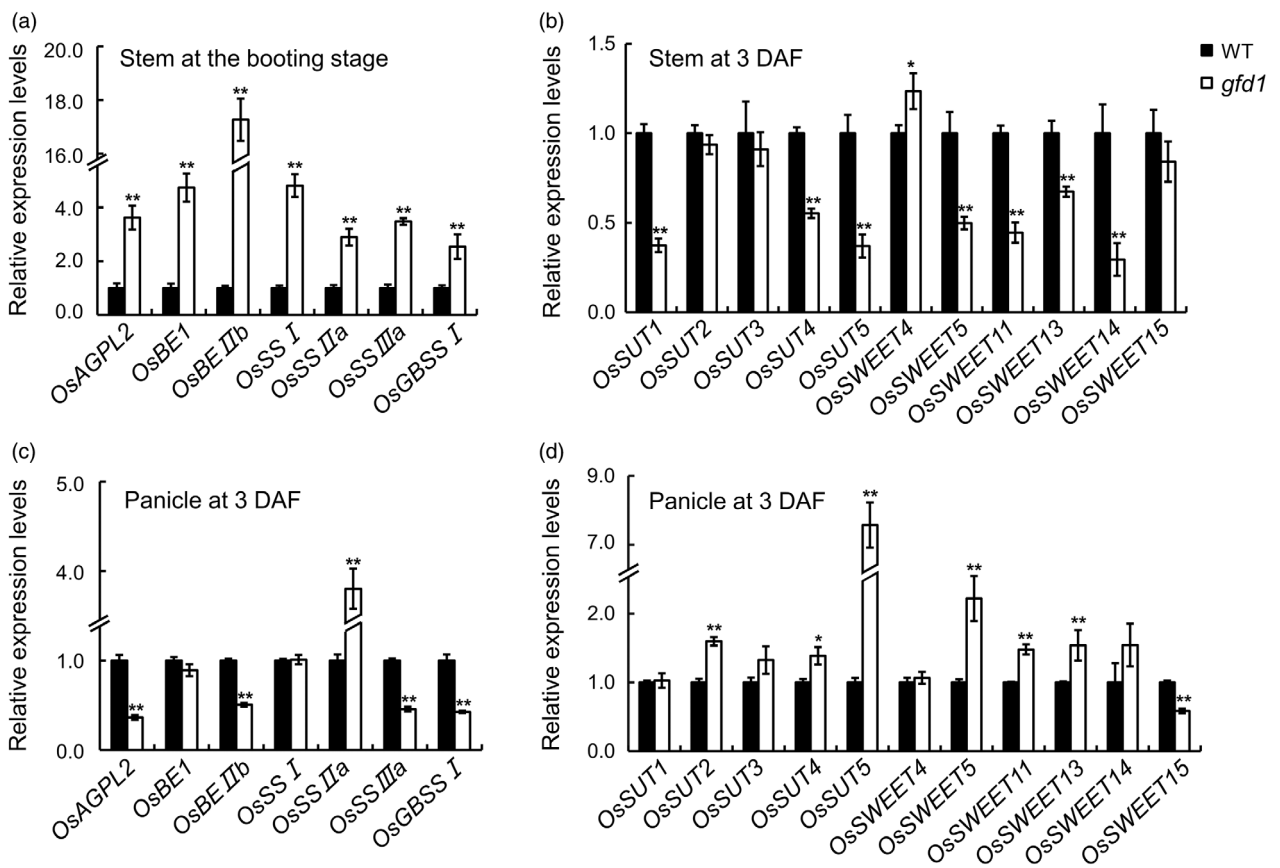

Figure 6 Expression analysis of starch synthesis and sugar transporter genes. *OsAGPL2* is an AGP large subunits gene; *OsBE1* and *OsBEIIb* are starch branching enzyme genes; *OsSSI*, *OsSSIIa* and *OsSSIIIa* are amylopectin synthesis genes; *OsGBSSI* is an amylose starch synthase gene; *OsSUT1-5*, *OsSWEET4*, *OsSWEET5*, *OsSWEET11*, *OsSWEET13*, *OsSWEET14* and *OsSWEET15* are sugar transporter genes. (a) Expression analyses of starch synthesis genes in the stem at the booting stage. (b) Expression analyses of sugar transporter genes in the stem at 3 days after fertilization (DAF). (c, d) Expression analyses of starch synthesis (c) and sugar transporter (d) genes in the panicle at 3 DAF. Data are given as the means ± SD from at least three replications. Asterisks indicate statistically significant differences between WT and *gfd1* by Student's *t*-test analysis (*$P < 0.05$; **$P < 0.01$).

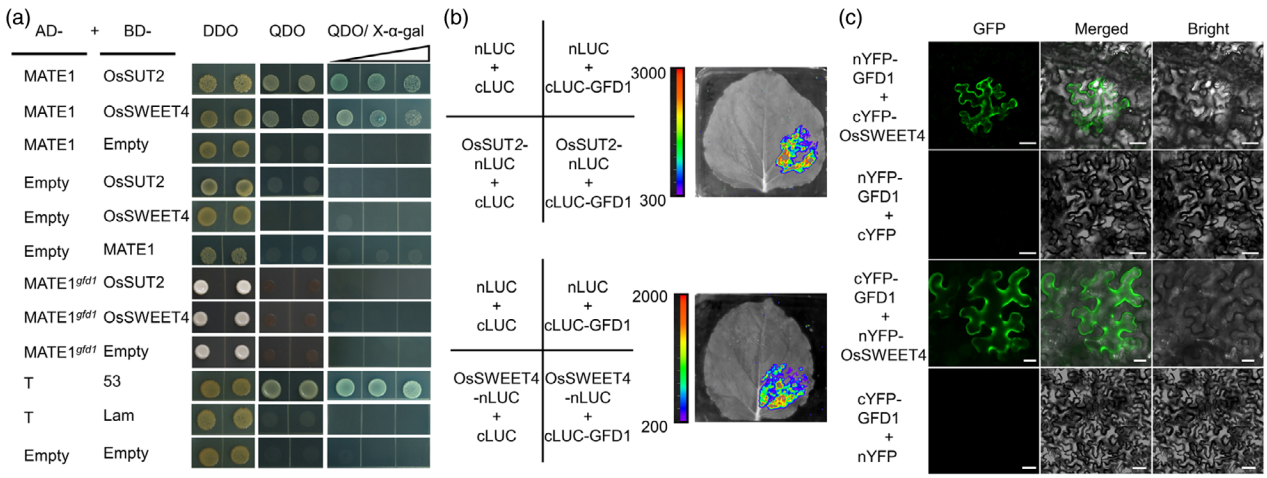

Figure 7 GFD1 could interact with OsSUT2 and OsSWEET4. (a) Yeast two-hybrid assays (Y_2H) showed that MATE1 could interact with OsSUT2 and OsSWEET4. Serial dilutions (1, 1/10, 1/100) of yeast transformant were plated onto the medium of QDO/X-α-gal for further screening. Co-transformation of pGADT7-T (T) and pGBKT7-53 (53) was used as the positive control. The transformant of pGADT7-T (T) and pGBKT7-lam (lam), pGADT7 (AD) and pGBKT7 (BD) were used as the two negative controls. DDO, SD/-Leu/-Trp; QDO, SD/-Leu/-Trp/-Ade/-His. (b) LCI assay of GFD1 with OsSUT2 (up) or OsSWEET4 (down) in tobacco leaves. Coloured scale bars indicate the luminescence intensity in counts per second (cps). (c) Bimolecular fluorescence complementation assay analysis. nYFP-GFD1 with cYFP-OsSWEET4, cYFP-GFD1 with nYFP-OsSWEET4 were co-transformed into tobacco leaves. nYFP, N-terminal YFP; cYFP, C-terminal YFP. nYFP-GFD1 with cYFP, cYFP-GFD1 with nYFP served as negative controls. Scale bars, 20 μm.

and OsSWEET4, fusing BD vectors. The results showed that the mutant MATE1^{gfd1} domain could not interact with OsSUT2 and OsSWEET4 in yeast, suggesting that a single mutant from Glu to Lys could block the interaction between GFD1 and OsSUT2/OsSWEET4 (Figure 7a).

Next, we tested whether GFD1 interacted with OsSUT2 or OsSWEET4 in plant cells. LCI assays were applied in *N. benthamiana* leaves (Hu *et al.*, 2019). Apparent LUC activity was observed when cLUC-GFD1 was co-transformed with OsSUT2-nLUC or OsSWEET4-nLUC (Figure 7b). Moreover, bimolecular fluorescence complementation assay (BiFC) assays showed that OsSWEET4 and GFD1 could be associated with the plasma membrane in *N. benthamiana* leaf cells (Figure 7c). Consequently, our data suggested that GFD1 could interact with OsSUT2 and OsSWEET4 *in vitro* and *in vivo*.

Genetic relationship analysis of *GFD1* and *OsSWEET4/OsSUT2*

GFD1 could interact with OsSWEET4 and OsSUT2, mediate carbohydrate partitioning and affect grain-filling duration, grain size and number per panicle in rice. These results lead us to find out the genetic relationship between *GFD1* and *OsSWEET4/OsSUT2*. Therefore, we generated single knockout mutants *ossweet4* and *ossut2*, and double-mutant *gfd1*^{ZH11} *ossweet4* and *gfd1*^{ZH11} *ossut2* in ZH11 and *gfd1*^{ZH11} (KO2-1) by CRISPR/Cas9 technology (Figure S12). Then, we planted ZH11, *gfd1*^{ZH11}, *ossweet4*, *ossut2*, *gfd1*^{ZH11} *ossweet4* and *gfd1*^{ZH11} *ossut2* in the experimental fields in Wenjiang, Chengdu (Figure 8).

It was reported that OsSWEET4 acted as a switch controlling sugar transport from the maternal phloem into the endosperm at the basal endosperm transfer layer (Sosso *et al.*, 2015). Our *ossweet4* mutant was also defective in seed filling. Moreover, the double-mutant *gfd1*^{ZH11} *ossweet4* showed a similar inferior grain-filling variation with *ossweet4*, indicating that the regulating function of GFD1 might be OsSWEET4-dependent in sugar transport and grain-filling process (Figure 8a). Additionally, *ossweet4* and *ossut2* could reduce grain number per panicle in ZH11 and *gfd1*^{ZH11} background (Figure 8b,e–g), suggesting that the three transporters coordinate controlled grain number per panicle in rice.

Consistent with the previous report, *ossut2* mutant exhibited a growth retardation phenotype (Eom *et al.*, 2011). The single-mutant *ossut2* did not change the grain-filling duration (Figure 8k), while the double-mutant *gfd1*^{ZH11} *ossut2* showed a longer grain-filling duration as *gfd1*, and the seed at 33 DAF was greener than *ossut2* (Figure 8j). Furthermore, a substantial reduction in grain weight of double-mutant *gfd1*^{ZH11} *ossut2* was found during the whole grain-filling process (Figure 8k). As the double-mutant *gfd1*^{ZH11} *ossut2* showed a medial grain size between *gfd1*^{ZH11} and *ossut2*, *GFD1* and *OsSUT2* were antagonists in grain size regulation (Figure 8c,d,h,i). Therefore, the less grain weight was completely dependent on the grain-filling ability loss in the double-mutant *gfd1*^{ZH11} *ossut2*. These results suggested that, in the *gfd1* background, *ossut2* severely affected grain-filling ability, implying an enhanced relationship between *GFD1* and *OsSUT2* in the grain-filling process.

Discussion

MATE transporter GFD1 controls the grain-filling duration in rice

In rice, grain filling is essential to determine the accumulation rate and duration of storage compounds in the grain and also has a crucial influence on rice's final yield and quality (Nagata *et al.*, 2015; Takai *et al.*, 2005; Upadhyay *et al.*, 2019; Wang *et al.*, 2008). So far, only a few grain-filling genes have been identified, but most of these genes do not remarkably affect the grain-filling duration (Hirose *et al.*, 2002; Liu *et al.*, 2019; Wang *et al.*, 2008; Wei *et al.*, 2017; Xiong *et al.*, 2019). Besides, grain-filling duration is also an important agronomic trait that defines maturity duration for seasonal and regional adaptation after the heading date in rice (Chen *et al.*, 2022; Fang *et al.*, 2019; Sun

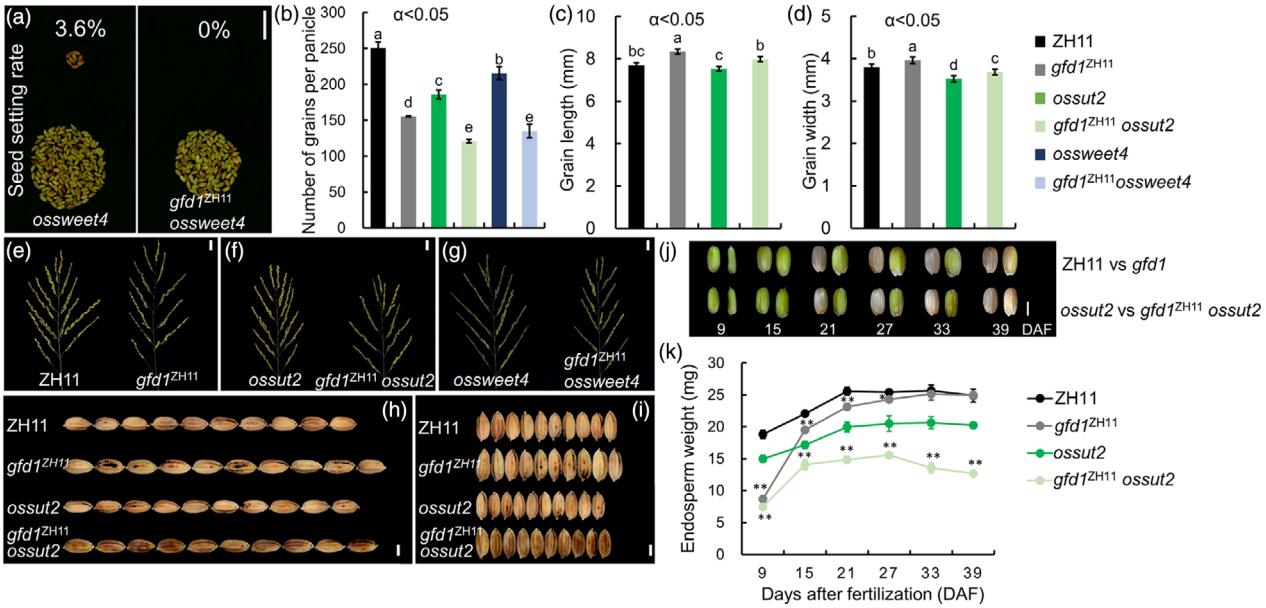

Figure 8 Genetic analysis of *GFD1*, *OsSUT2* and *OsSWEET4*. (a) Comparison of seed setting rate of *ossweet4* and *gfd1 ossweet4*. Scale bars, 2 cm. (b, e, f and g) Comparison of grain numbers per panicle of ZH11, *gfd1*^{ZH11}, *ossut2*, *gfd1*^{ZH11} *ossut2*, *ossweet4* and *gfd1*^{ZH11} *ossweet4*. Scale bars, 2 cm. (c, d, h and i) Comparison of grain length and grain width of ZH11, *gfd1*^{ZH11}, *ossut2* and *gfd1*^{ZH11} *ossut2*. Scale bars, 3 mm. (j) Caryopsis comparison at 9, 15, 21, 27, 33 and 39 day after fertilization (DAF) in ZH11 (up, left), *gfd1*^{ZH11} (up, right), *ossut2* (down, left) and *gfd1*^{ZH11} *ossut2* (down, right). Scale bars, 3 mm. (k) Caryopsis weight at various stages of grain filling in ZH11, *gfd1*^{ZH11}, *ossut2* and *gfd1*^{ZH11} *ossut2*. Details of KO4-3 (*ossut2*), KO5-7 (*gfd1*^{ZH11} *ossut2*), KO6-1 (*ossweet4*), KO7-3 (*gfd1*^{ZH11} *ossweet4*) are showed in Figure S12. The letters a, b, c, d and e in (b–d) indicate significant differences at $P < 0.05$ according to one-way ANOVA test with Tukey correction. Asterisks in (k) indicate statistically significant differences Student's *t*-test analysis (**$P < 0.01$).

et al., 2014, 2021; Zhao *et al*., 2018; Zhou *et al*., 2021). On the contrary, MATE transporters belong to one of the largest transporter families and are involved in various physiological and developmental functions (Takanashi *et al*., 2014; Upadhyay *et al*., 2019; Wang *et al*., 2016). In our study, though the grain weight of *gfd1* was nearly the same as that of the WT, the grain-filling duration was largely prolonged. Hence, we build a relationship between the grain-filling duration and a MATE transporter GFD1.

GFD1 might tune the transport rate of OsSWEET4

When arrived at the grain, the apoplastic sucrose is split by cell wall-bound invertases (such as OsGIF1) into glucose and fructose, which are subsequently uptake into the endosperm by hexose transporters. OsSWEET4, which was proven as a hexose transporter at the basal endosperm transfer layer and localized on the plasma membrane, is required for this uptake (Sosso *et al*., 2015). Our study verified that *GFD1* could also express in the basal endosperm transfer layer and localized on the plasma membrane. Besides, *ossweet4* exhibited defective grain-filling phenotypic variation, while *gfd1* showed longer grain-filling duration and lower grain-filling rate. Therefore, GFD1 and OsSWEET4 might interact for hexose transportation together. We designed four experiments and proved our assumption. First, yeast two-hybrid assays showed that GFD1 could interact with OsSWEET4. Second, the interaction was further confirmed by the LCI assay. Third, BiFC results showed that GFD1 interacted with OsSWEET4 in the plasma membrane. Finally, the double-mutant *gfd1*^{ZH11} *ossweet4* showed a similar grain-filling defect just as *ossweet4*. Therefore, it seems that *OsSWEET4* is epistatic to *GFD1*. OsSWEET4 acts as an on/off switch of grain filling, while GFD1 is the regulator of this switch through physical interaction with OsSWEET4, controlling the valve of the switch and tuning the flow rate of hexose in the basal endosperm transfer layer.

GFD1 involves in stem starch reserves

The plant stem can act as an intermediate storage sink organ of starch. In rice, 24–27% of grain carbohydrate originates from stem starch reserves (CocK and Yoshida, 1972), making stem starch a significant carbohydrate source in the grain-filling process (Scofield *et al*., 2007b). Interestingly, cultivated rice Nipponbare utilizes stem starch more than *Oryza australiensis* at the grain-filling stage and produces a higher grain yield (Mathan *et al*., 2021a; Wang *et al*., 2020). However, the mechanisms for sucrose and starch assimilating into and out of the stem are rarely understood (Scofield *et al*., 2007b). Our research on GFD1 provided some clues. Compared with WT, starch content and SG density of *gfd1* was higher in the stem but not in the leaf, especially at the grain-filling stage, suggesting that GFD1 could participate in starch accumulation in the stem. However, though the starch content was still a little higher in *gfd1* stem after the grain-filling stage, most SGs in WT and *gfd1* stems disappeared after the completion of grain filling, suggesting that the SGs accumulated in *gfd1* stems might be due to its slow grain-filling rate.

GFD1 may be an enhancer of *OsSUT2*

A previous study showed that *ossut2* significantly reduced sugar exportability and likely interfered with sucrose translocation to sink organs (Sun *et al*., 2008). Furthermore, OsSUT2 could be involved in unloading an enormous amount of sucrose being received in the stem (Wang *et al*., 2020). In our study, the single-mutant *ossut2* did not exhibit grain-filling defect phenotypes.

However, the double-mutant *gfd1*^{ZH11} *ossut2* exhibited severer grain-filling variants, a prolonged grain-filling duration and a substantial reduction in grain weight during the whole grain-filling process. Compared with *ossut2*, the grain size in double-mutant *gfd1*^{ZH11} *ossut2* is larger. Still, the grain weight is significantly lower, which is different from both *ossut2* and *gfd1* single mutants, suggesting that functional *GFD1* could partly compensate for the loss of function *OsSUT2*. Therefore, *GFD1* and *OsSUT2* may act on the same pathway, and *GFD1* may be an enhancer of *OsSUT2* in grain-filling process.

Some clues on sugar transporter interactome

Membranes contain thousands of proteins whose biochemical or physiological functions have not been identified experimentally. The transport activity of many transporters depends on the interactions of membrane proteins (Lalonde *et al*., 2010). However, most of the putative protein–protein interactions were previously unknown. Identifying genetic and molecular interactions is a hopeful way to identify membrane protein functions (Boone *et al*., 2007; Jones *et al*., 2014; Jonikas *et al*., 2009; Lalonde *et al*., 2008). MATEs are initially classified as members of the Na^+- or H^+-coupled transporters in the major facilitator superfamily (MFS), which is one of the two largest membrane transporter families on the earth (Pao *et al*., 1998; Upadhyay *et al*., 2019). Plant sugar SWEETs and SUTs proteins are initially attributed to MFS (Marger and Saier, 1993; Wipf *et al*., 2021). Interestingly, we provided evidence that MATE transporter GFD1 could interact with OsSUT2 and OsSWEET4 and assist them in sugar transport. Though GFD1 and OsSWEET4 are associated with the plasma membrane, the subcellar locations of OsSUT2 and GFD1 are different. GFD1 protein was localized on the plasma membrane and in the Golgi apparatus, while OsSUT2 was tonoplast-localized.

In eukaryotic cells, proteins transport across organelles such as the plasma membrane, the Golgi apparatus and vacuoles by membrane trafficking, which is essential for normal cellular functions (Shimizu *et al*., 2021). In our subcellular localization experiments, we found a large variation in the number and size of the punctate signals of GFD1. As some punctate signals are localized in Golgi, others are still out of the Golgi, suggesting other possible subcellular localizations of GFD1. These punctate apparatuses might translocate GFD1 to the tonoplast where OsSUT2 is localized. Exploring this cross-organelle interaction mechanism will give a new vision to sugar transporter interactome research.

GFD1 takes part in multiple regulatory pathways

Interacting with OsSWEET4 and OsSUT2 could not fully explain all the varied phenotypes of *gfd1*. More regulation pathways need to be explored in future studies. Sucrose metabolism plays a pivotal role in synthesizing essential compounds for plant growth. On the contrary, sugars could also act as signals to regulate meristem activity, flowering, inflorescence branching, tillering and so on (Ruan, 2014). The disordered sugar distribution in *gfd1* might also affect sugar signals distributing for plant development regulation. Additionally, we cannot rule out that GFD1 might involve other substances' transportation.

Materials and methods

Plant materials and growth conditions

The *gfd1* mutant was obtained by screening the EMS mutagenesis library of *indica* rice cv. Gang46B (G46B). F_2 population (*gfd1* × G46B) was used for genetic analysis. F_2 population of *gfd1* × ZH11 (Zhonghua11, a *japonica* variety), and B_2F_2 and B_4F_2 populations by backcrossing with ZH11 were used for gene mapping.

Rice seedlings for generating protoplast cells were grown in the dark at 28°C, and *N. benthamiana* plants were grown in a culture room at 23°C with a 16-h light and 8-h dark photoperiod. Other plant materials were grown under normal conditions in Sichuan Agriculture University's experimental fields in Wenjiang, Chengdu, China (Wang *et al*., 2010).

Grain-filling duration investigation

To obtain fertilized spikelets on the same day, we cut off the pollinated spikelets in the early morning and unpollinated spikelets at dusk in 1 day. The spikelets still in the panicle were used for grain-filling duration determination. For WT and *gfd1*, fresh grains were randomly collected every 3 days since 3 DAF. For complementation, knockout of *GFD1* analysis and the double-mutant *gfd1*^{ZH11} *ossut2* analysis, the fresh grains were randomly collected every 6 days since 9 DAF. Then, the fresh caryopses were weighed. Three biological replicates were performed with no less than 30 grains per replicate.

Microscopy

Scanning electron microscopy was performed according to a modified method using an Apreo S scanning electron microscope (Thermo Fisher, Waltham, Massachusetts, United States) (Kang *et al*., 2006). For SG detection in the internode, paraffin sections were made as described by Li *et al*. (2009a,2009b). The paraffin sections were stained with I_2-KI and observed under a light microscope (Nikon DS-U3; Nikon, Minato City, Tokyo, Japan) (Peng *et al*., 2014). For transmission electron microscopy analysis, leaves were treated in 3% glutaraldehyde and then fixed in 1% osmium tetroxide. After dehydrating in a gradient acetone series, the leaf sections were embedded in Epon812 medium for thin sectioning. Uranyl acetate and Reynolds' lead citrate were used to stain the thin sectioning, and an H-600 IV transmission electron microscope was used to assess the picture (Hitachi, Chiyoda City, Tokyo, Japan) (Li *et al*., 2015).

Measurement of sugar and starch

Mature grains of WT and *gfd1* were shelled and ground into powder, respectively. Leaves (the top-three leaves), stems or developing grains of WT and *gfd1* were harvested at the heading stage, 9 DAF, 15 DAF, and after the grain-filling stage, and then dried at 65°C for heat-inactivation. The above samples' total starch content was measured according to the manufacturer's protocol with a starch assay kit (BC0705; Solarbio, Fengtai District, Beijing, China). Sucrose, glucose and fructose contents were determined using soluble sugar assay kits BC2465, BC2505 and BC2455 (Solarbio, Fengtai District, Beijing, China). All analyses were repeated with three biological replicates.

Map-based cloning

For map-based cloning, F_2 population crossing by *gfd1* and ZH11, and subsequent B_2F_2, B_4F_2 generation populations were constructed. A total of 2157 slower grain-filling homozygous individuals were collected in 3 years (2011–2014) in Wenjiang, Chengdu, China. We screened and got more than 100 polymorphic SSR markers distributed over the 12 chromosomes between *gfd1* and ZH11. Insertion/deletion (InDel) and SNP markers were developed based on nucleotide polymorphisms between Nipponbare and *indica* rice cv 9311 reference genomes in the corresponding regions. All the primers are listed in Table S1.

Vector construction and rice transformation

For complement of *gfd1*, the whole genomic fragment of WT (G46B) *GFD1* containing 3-kb native promoter was inserted into pCAMBIA1300 vector (Table S1) and then transformed into the near-isogenic line of *gfd1* in the ZH11 background (NIL^{ZH11}).

According to the previous method, CRISPR/Cas9 vector construction was performed (Cong *et al.*, 2013). The targeting sequences of *GFD1* (two targets, SG1: GGACGCGGCGCAGACGTTCG; SG2: CCGGCTACTCGGTGCTCTCC), *OsSUT2* (SG3: CAAGTCTGCCTTTCTACTTC) and *OsSWEET4* (SG4: ACGTTCATACGGATCTGGA) were synthesized and annealed to form the oligo adaptors. Agrobacterium-mediated transformation was performed as described previously (Hiei *et al.*, 1994). Finally, *GFD1* was knockout in ZH11 (two targets, SG1 and SG2) and Nipponbare (one target, SG2). *OsSUT2* and *OsSWEET4* were knockout in ZH11 and KO2-1 ($gfd1^{ZH11}$, Figures S3, S12) to generate single and double mutants. All the primers are listed in Table S1.

RNA isolation and quantitative RT-PCR

According to the product manual, total RNA was extracted using an RNA isolater (Total RNA Extraction Reagent, R401-01; Vazyme, Red Maple Technology Industrial Park, Nanjing, China). Reverse transcription of total RNA (~2 μg) was performed using HiScript III RT SuperMix for qPCR (+gDNA wiper) (R323-01; Vazyme, Red Maple Technology Industrial Park, Nanjing, China). The qRT-PCR analysis was performed on a CFX96 real-time PCR system (Bio-Rad, Hercules, California, United States) with ChamQ Universal SYBR qPCR Master Mix (Q711-03; Vazyme, Red Maple Technology Industrial Park, Nanjing, China). The *Actin1* gene was used as the internal control (Li *et al.*, 2015). The primers used here are listed in Table S1.

Histochemical GUS analysis

The 1.6-kb promoter of *GFD1* was amplified from G46B and cloned into the pCAMBIA1391Z (Table S1). The resulting vector Pro*GFD1*:GUS was transformed into ZH11 by the Agrobacterium-mediated transformation method (Hiei *et al.*, 1994). Histochemical GUS assay was performed as described previously (Jefferson *et al.*, 1987). The tissues for detection were soaked in GUS staining solution, incubated at 37°C for 12–15 h and faded by Alcohol: acetic mixture (3:1) for observation. For microscopic examination, the developing caryopsis in 30 DAF was fixed in FAA after GUS staining for paraffin section making (Li *et al.*, 2009b) and then observed using a Nikon DS-U3 light microscope (Nikon).

In situ hybridization

The stem at the booting stage and the caryopsis at 9 DAF were used for *in situ* hybridization detection following the method depicted by Kouchi and Hata (Kouchi and Hata, 1993). In brief, the *GFD1*-specific probe (Table S1) was labelled using Digoxigenin. After fixation, dehydration, sectioning, pre-hybridization, hybridization, anti-DIG-AP and BCIP/NBT chromogenic solution addition, rinsing and sealing, the samples were observed and photographed by a Nikon DS-U3 light microscope (Nikon).

Subcellular localization of GFD1

Green fluorescent protein (GFP) was fused to N- and C-terminus of full-length *GFD1* CDS (coding sequence) driven by cauliflower mosaic virus (CaMV) 35 S promoter (Table S1). Then, the two fusion constructs, GFP-GFD1 and GFD1-GFP, were transformed into rice protoplasts separately following the method described by Chen *et al.* (2006). Meanwhile, OsRAC3-mRFP (monomeric red fluorescent protein) was used as a plasma membrane marker (Chen *et al.*, 2010). Man49-mRFP (Nelson *et al.*, 2007) and ERD2-mRFP (Montesinos *et al.*, 2014) were used as Golgi markers. These makers were co-transformed into rice protoplasts or *N. benthamiana* leaves with GFD1-GFP (Li *et al.*, 2009a). Fluorescence signals were observed under a confocal laser scanning microscope (Nikon A1; Nikon).

Yeast two-hybrid assay

Yeast two-hybrid (Y_2H) assay was performed using the Y_2H Gold-Gal4 system (Clontech, http://www.clontech.com). Full-length CDS, the containing domains (MATE1, MATE2 and the mutant $MATE1^{gfd1}$) of *GFD1*, and the sugar transporters CDS (*OsSUT1-5*, *OsSWEET4*, *OsSWEET11* and *OsSWEET15*), were cloned into pGADT7 (AD) and pGBKT7 (BD), respectively. Yeast transformations were completed following the manufacturer's instructions (Clontech) and cultured on SD/-Trp-Leu or SD/-Trp-Leu-His-Ade medium containing X-α-gal at 30°C in the dark for about 3 days. Primers used are given in Table S1.

LCI assay

Split-luciferase complementation (LCI) assay was performed as described previously (Hu *et al.*, 2019). The full-length CDS of *GFD1, OsSUT2* and *OsSWEET4* was amplified and fused with luciferase (Table S1). The final constructs were introduced into *Agrobacterium tumefaciens* strain EHA105 and pairwise infiltrated the *N. benthamiana* leaves. Then, the leaves were stained using Beetle Luciferin, Potassium Salt kit (E1601; Promega, Madison, Wisconsin, United States) and placed into NightOWLIIILB 983 in *vivo* imaging system (Berthold, Bad Wildbad, Germany). The interaction was determined based on the bioluminescence signal intensity acquired by IndiGO software.

BiFC assay

For BiFC, fusion vectors of GFD1 or OsSWEET4 were constructed using the binary BiFC vectors pSPYNE (nYFP) and pSPYCE (cYFP), respectively (Table S1). Bimolecular fluorescence complementation assay analysis was performed in the leaf epidermal cells of *N. benthamiana*, as previously described (Waadt and Kudla, 2008). The YFP fluorescence was observed using a Nikon A1 laser scanning confocal microscope (Nikon, Minato City, Tokyo, Japan).

Acknowledgements

This study was supported by grants from the National Natural Science Foundation of China (91335107, 91735303, 32172022, 31371602 and 31401358) and the Sichuan Science and Technology Program (2020YJ0408).

Conflicts of interest statement

The authors declare no conflict of interest.

Author contributions

CS, PW and XD planned and designed the research. CS, YW, XY, LT, CW, JL, CC, HZ, CH, CL, QW, KZ, WZ and BY performed experiments and conducted fieldwork. CS, YW, XY, LT, CW, JL, SL, JZ, YS, WL, PW and XD analysed data. CS, YW, YZ and XD wrote the manuscript. CS, YW, XY, LT, CW and JL contributed equally.

References

Alexandratos, N. and Bruinsma, J. (2012) *World agriculture towards 2030/2050: the 2012 revision*.

Aoki, N., Hirose, T., Scofield, G.N., Whitfeld, P.R. and Furbank, R.T. (2003) The sucrose transporter gene family in rice. *Plant Cell Physiol.* **44**, 223–232.

Bihmidine, S., Baker, R.F., Hoffner, C. and Braun, D.M. (2015) Sucrose accumulation in sweet sorghum stems occurs by apoplasmic phloem unloading and does not involve differential Sucrose transporter expression. *BMC Plant Biol.* **15**, 186.

Boone, C., Bussey, H. and Andrews, B.J. (2007) Exploring genetic interactions and networks with yeast. *Nat. Rev. Genet.* **8**, 437–449.

Chen, S., Tao, L., Zeng, L., Vega-Sanchez, M.E., Umemura, K. and Wang, G.L. (2006) A highly efficient transient protoplast system for analyzing defence gene expression and protein-protein interactions in rice. *Mol. Plant Pathol.* **7**, 417–427.

Chen, L., Shiotani, K., Togashi, T., Miki, D., Aoyama, M., Wong, H.L., Kawasaki, T. *et al*. (2010) Analysis of the Rac/Rop small GTPase family in rice: expression, subcellular localization and role in disease resistance. *Plant Cell Physiol.* **51**, 585–595.

Chen, L.Q., Qu, X.Q., Hou, B.H., Sosso, D., Osorio, S., Fernie, A.R. and Frommer, W.B. (2012) Sucrose efflux mediated by SWEET proteins as a key step for phloem transport. *Science* **335**, 207–211.

Chen, R., Deng, Y., Ding, Y., Guo, J., Qiu, J., Wang, B., Wang, C. *et al*. (2022) Rice functional genomics: decades' efforts and roads ahead. *Sci. China Life Sci.* **65**, 33–92.

CocK, J.H. and Yoshida, S. (1972) Accumulation of ^{14}C-labelled carbohydrate before flowering and its subsequent redistribution and respiration in the rice plant. *Japanese J. Crop Sci.* **41**, 226–234.

Cong, L., Ran, F.A., Cox, D., Lin, S., Barretto, R., Habib, N., Hsu, P.D. *et al*. (2013) Multiplex genome engineering using CRISPR/Cas systems. *Science* **339**, 819–823.

Durand, M., Mainson, D., Porcheron, B., Maurousset, L., Lemoine, R. and Pourtau, N. (2018) Carbon source-sink relationship in *Arabidopsis thaliana*: the role of sucrose transporters. *Planta* **247**, 587–611.

Eom, J.S., Cho, J.I., Reinders, A., Lee, S.W., Yoo, Y., Tuan, P.Q., Choi, S.B. *et al*. (2011) Impaired function of the tonoplast-localized sucrose transporter in rice, OsSUT2, limits the transport of vacuolar reserve sucrose and affects plant growth. *Plant Physiol.* **157**, 109–119.

Fang, J., Zhang, F., Wang, H., Wang, W., Zhao, F., Li, Z., Sun, C. *et al*. (2019) Ef-cd locus shortens rice maturity duration without yield penalty. *Proc. Natl. Acad. Sci. U. S. A.* **116**, 18717–18722.

Furbank, R.T., Scofield, G.N., Hirose, T., Wang, X.-D., Patrick, J.W. and Offler, C.E. (2001) Cellular localisation and function of a sucrose transporter OsSUT1 in developing rice grains. *Funct. Plant Biol.* **28**, 1187–1196.

Hiei, Y., Ohta, S., Komari, T. and Kumashiro, T. (1994) Efficient transformation of rice (*Oryza sativa* L.) mediated by Agrobacterium and sequence analysis of the boundaries of the T-DNA. *Plant J.* **6**, 271–282.

Hirose, T., Takano, M. and Terao, T. (2002) Cell wall invertase in developing rice caryopsis: molecular cloning of OsCIN1 and analysis of its expression in relation to its role in grain filling. *Plant Cell Physiol.* **43**, 452–459.

Hirose, T., Zhang, Z., Miyao, A., Hirochika, H., Ohsugi, R. and Terao, T. (2010) Disruption of a gene for rice sucrose transporter, OsSUT1, impairs pollen function but pollen maturation is unaffected. *J. Exp. Bot.* **61**, 3639–3646.

Hu, B., Jiang, Z., Wang, W., Qiu, Y., Zhang, Z., Liu, Y., Li, A. *et al*. (2019) Nitrate-NRT1.1B-SPX4 cascade integrates nitrogen and phosphorus signalling networks in plants. *Nat Plants* **5**, 401–413.

Jefferson, R.A., Kavanagh, T.A. and Bevan, M.W. (1987) GUS fusions: beta-glucuronidase as a sensitive and versatile gene fusion marker in higher plants. *EMBO J.* **6**, 3901–3907.

Jones, A.M., Xuan, Y., Xu, M., Wang, R.S., Ho, C.H., Lalonde, S., You, C.H. *et al*. (2014) Border control—a membrane-linked interactome of Arabidopsis. *Science* **344**, 711–716.

Jonikas, M.C., Collins, S.R., Denic, V., Oh, E., Quan, E.M., Schmid, V., Weibezahn, J. *et al*. (2009) Comprehensive characterization of genes required for protein folding in the endoplasmic reticulum. *Science* **323**, 1693–1697.

Julius, B.T., Leach, K.A., Tran, T.M., Mertz, R.A. and Braun, D.M. (2017) Sugar transporters in plants: new insights and discoveries. *Plant Cell Physiol.* **58**, 1442–1460.

Kang, J., Jain, M., Wilkinson, D.S. and Embury, J.D. (2006) Microscopic strain mapping using scanning electron microscopy topography image correlation at large strain. *J. Strain Analysis Eng. Design* **40**, 559–570.

Kouchi, H. and Hata, S. (1993) Isolation and characterization of novel nodulin cDNAs representing genes expressed at early stages of soybean nodule development. *Mol. Gen. Genet.* **238**, 106–119.

Krishnan, S. and Dayanandan, P. (2003) Structural and histochemical studies on grain-filling in the caryopsis of rice (*Oryza sativa* L.). *J. Biosci.* **28**, 455–469.

Kuroda, T. and Tsuchiya, T. (2009) Multidrug efflux transporters in the MATE family. *Biochim. Biophys. Acta* **1794**, 763–768.

Lalonde, S., Ehrhardt, D.W., Loque, D., Chen, J., Rhee, S.Y. and Frommer, W.B. (2008) Molecular and cellular approaches for the detection of protein-protein interactions: latest techniques and current limitations. *Plant J.* **53**, 610–635.

Lalonde, S., Sero, A., Pratelli, R., Pilot, G., Chen, J., Sardi, M.I., Parsa, S.A. *et al*. (2010) A membrane protein/signaling protein interaction network for Arabidopsis version AMPv2. *Front. Physiol.* **1**, 24.

Li, M., Xiong, G., Li, R., Cui, J., Tang, D., Zhang, B., Pauly, M. *et al*. (2009a) Rice cellulose synthase-like D4 is essential for normal cell-wall biosynthesis and plant growth. *Plant J.* **60**, 1055–1069.

Li, S., Qian, Q., Fu, Z., Zeng, D., Meng, X., Kyozuka, J., Maekawa, M. *et al*. (2009b) Short panicle1 encodes a putative PTR family transporter and determines rice panicle size. *Plant J.* **58**, 592–605.

Li, C., Hu, Y., Huang, R., Ma, X., Wang, Y., Liao, T., Zhong, P. *et al*. (2015) Mutation of FdC2 gene encoding a ferredoxin-like protein with C-terminal extension causes yellow-green leaf phenotype in rice. *Plant Sci.* **238**, 127–134.

Li, S., Wei, X., Ren, Y., Qiu, J., Jiao, G., Guo, X., Tang, S. *et al*. (2017) OsBT1 encodes an ADP-glucose transporter involved in starch synthesis and compound granule formation in rice endosperm. *Sci. Rep.* **7**, 1–13.

Li, P., Wang, L.H., Liu, H.B. and Yuan, M. (2022) Impaired SWEET-mediated sugar transportation impacts starch metabolism in developing rice seeds. *Crop J.* **10**, 98–108.

Liu, E., Zeng, S., Zhu, S., Liu, Y., Wu, G., Zhao, K., Liu, X. *et al*. (2019) Favorable alleles of grain-filling RATE1 increase the grain-filling rate and yield of rice. *Plant Physiol.* **181**, 1207–1222.

Ma, L., Zhang, D., Miao, Q., Yang, J., Xuan, Y. and Hu, Y. (2017) Essential role of sugar transporter OsSWEET11 during the early stage of rice grain filling. *Plant Cell Physiol.* **58**, 863–873.

Marger, M.D. and Saier, M.H. (1993) A major superfamily of transmembrane facilitators that catalyse uniport, symport and antiport. *Trends Biochem. Sci.* **18**, 13–20.

Mathan, J., Singh, A. and Ranjan, A. (2021a) Sucrose transport and metabolism control carbon partitioning between stem and grain in rice. *J. Exp. Bot.* **72**, 4355–4372.

Mathan, J., Singh, A. and Ranjan, A. (2021b) Sucrose transport in response to drought and salt stress involves ABA-mediated induction of OsSWEET13 and OsSWEET15 in rice. *Physiol. Plant.* **171**, 620–637.

Matsukura, C., Saitoh, T., Hirose, T., Ohsugi, R., Perata, P. and Yamaguchi, J. (2000) Sugar uptake and transport in rice embryo. Expression of companion cell-specific sucrose transporter (OsSUT1) induced by sugar and light. *Plant Physiol.* **124**, 85–93.

Montesinos, J.C., Pastor-Cantizano, N., Robinson, D.G., Marcote, M.J. and Aniento, F. (2014) Arabidopsis p24δ5 and p24δ9 facilitate Coat Protein I-dependent transport of the K/HDEL receptor ERD2 from the Golgi to the endoplasmic reticulum. *Plant J.* **80**, 1014–1030.

Nagata, K., Yoshinaga, S., J-i, T. and Terao, T. (2015) Effects of dry matter production, translocation of nonstructural carbohydrates and nitrogen application on grain filling in rice cultivar Takanari, a cultivar bearing a large number of spikelets. *Plant Prod. Sci.* **4**, 173–183.

Nelson, B.K., Cai, X. and Nebenfuhr, A. (2007) A multicolored set of in vivo organelle markers for co-localization studies in Arabidopsis and other plants. *Plant J.* **51**, 1126–1136.

Omote, H., Hiasa, M., Matsumoto, T., Otsuka, M. and Moriyama, Y. (2006) The MATE proteins as fundamental transporters of metabolic and xenobiotic organic cations. *Trends Pharmacol. Sci.* **27**, 587–593.

Pao, S.S., Paulsen, I.T. and Saier, M.H., Jr. (1998) Major facilitator superfamily. *Microbiol. Mol. Biol. Rev.* **62**, 1–34.

Peng, C., Wang, Y., Liu, F., Ren, Y., Zhou, K., Lv, J., Zheng, M. *et al*. (2014) FLOURY ENDOSPERM6 encodes a CBM48 domain-containing protein involved in compound granule formation and starch synthesis in rice endosperm. *Plant J.* **77**, 917–930.

Ruan, Y.L. (2014) Sucrose metabolism: gateway to diverse carbon use and sugar signaling. *Annu. Rev. Plant Biol.* **65**, 33–67.

Scofield, G.N., Aoki, N., Hirose, T., Takano, M., Jenkins, C.L. and Furbank, R.T. (2007a) The role of the sucrose transporter, OsSUT1, in germination and early seedling growth and development of rice plants. *J. Exp. Bot.* **58**, 483–495.

Scofield, G.N., Hirose, T., Aoki, N. and Furbank, R.T. (2007b) Involvement of the sucrose transporter, OsSUT1, in the long-distance pathway for assimilate transport in rice. *J. Exp. Bot.* **58**, 3155–3169.

Shimizu, Y., Takagi, J., Ito, E., Ito, Y., Ebine, K., Komatsu, Y., Goto, Y. *et al*. (2021) Cargo sorting zones in the trans-Golgi network visualized by super-resolution confocal live imaging microscopy in plants. *Nat. Commun.* **12**, 1–14.

Siao, W., Chen, J.Y., Hsiao, H.H., Chung, P. and Wang, S.J. (2011) Characterization of OsSUT2 expression and regulation in germinating embryos of rice seeds. *Rice* **4**, 39–49.

Sosso, D., Luo, D., Li, Q.B., Sasse, J., Yang, J., Gendrot, G., Suzuki, M. *et al*. (2015) Seed filling in domesticated maize and rice depends on SWEET-mediated hexose transport. *Nat. Genet.* **47**, 1489–1493.

Sturm, A. and Tang, G.Q. (1999) The sucrose-cleaving enzymes of plants are crucial for development, growth and carbon partitioning. *Trends Plant Sci.* **4**, 401–407.

Sun, A.J., Xu, H.L., Gong, W.K., Zhai, H.L., Meng, K., Wang, Y.Q., Wei, X.L. *et al*. (2008) Cloning and expression analysis of rice sucrose transporter genes OsSUT2M and OsSUT5Z. *J. Integr. Plant Biol.* **50**, 62–75.

Sun, Y., Reinders, A., LaFleur, K.R., Mori, T. and Ward, J.M. (2010) Transport activity of rice sucrose transporters OsSUT1 and OsSUT5. *Plant Cell Physiol.* **51**, 114–122.

Sun, C., Chen, D., Fang, J., Wang, P., Deng, X. and Chu, C. (2014) Understanding the genetic and epigenetic architecture in complex network of rice flowering pathways. *Protein Cell* **5**, 889–898.

Sun, C., Zhang, K., Zhou, Y., Xiang, L., He, C., Zhong, C., Li, K. *et al*. (2021) Dual function of clock component OsLHY sets critical day length for photoperiodic flowering in rice. *Plant Biotechnol. J.* **19**, 1644–1657.

Takai, T., Fukuta, Y., Shiraiwa, T. and Horie, T. (2005) Time-related mapping of quantitative trait loci controlling grain-filling in rice (*Oryza sativa* L.). *J. Exp. Bot.* **56**, 2107–2118.

Takanashi, K., Shitan, N. and Yazaki, K. (2014) The multidrug and toxic compound extrusion (MATE) family in plants. *Plant Biotechnol.* **31**, 417–430.

Upadhyay, N., Kar, D., Deepak Mahajan, B., Nanda, S., Rahiman, R., Panchakshari, N., Bhagavatula, L. *et al*. (2019) The multitasking abilities of MATE transporters in plants. *J. Exp. Bot.* **70**, 4643–4656.

Waadt, R. and Kudla, J. (2008) In planta visualization of protein interactions using bimolecular fluorescence complementation (BiFC). *CSH Protoc* **2008**, pdb prot4995.

Wang, E., Wang, J., Zhu, X., Hao, W., Wang, L., Li, Q., Zhang, L. *et al*. (2008) Control of rice grain-filling and yield by a gene with a potential signature of domestication. *Nat. Genet.* **40**, 1370–1374.

Wang, P., Gao, J., Wan, C., Zhang, F., Xu, Z., Huang, X., Sun, X. *et al*. (2010) Divinyl chlorophyll(ide) a can be converted to monovinyl chlorophyll(ide) a by a divinyl reductase in rice. *Plant Physiol.* **153**, 994–1003.

Wang, L., Bei, X., Gao, J., Li, Y., Yan, Y. and Hu, Y. (2016) The similar and different evolutionary trends of MATE family occurred between rice and *Arabidopsis thaliana*. *BMC Plant Biol.* **16**, 207.

Wang, G.Q., Li, H.X., Gong, Y.L., Yang, J.C., Yi, Y.K., Zhang, J.H. and Ye, N.H. (2020) Expression profile of the carbon reserve remobilization from the source to sink in rice in response to soil drying during grain filling. *Food Energy Security* **9**, e204.

Wei, X., Jiao, G., Lin, H., Sheng, Z., Shao, G., Xie, L., Tang, S. *et al*. (2017) GRAIN INCOMPLETE FILLING 2 regulates grain filling and starch synthesis during rice caryopsis development. *J. Integr. Plant Biol.* **59**, 134–153.

Wipf, D., Pfister, C., Mounier, A., Leborgne-Castel, N., Frommer, W.B. and Courty, P.E. (2021) Identification of putative interactors of Arabidopsis sugar transporters. *Trends Plant Sci.* **26**, 13–22.

Wu, Y., Lee, S.K., Yoo, Y., Wei, J., Kwon, S.Y., Lee, S.W., Jeon, J.S. *et al*. (2018) Rice transcription factor OsDOF11 modulates sugar transport by promoting expression of sucrose transporter and SWEET genes. *Mol. Plant* **11**, 833–845.

Xiong, Y., Ren, Y., Li, W., Wu, F., Yang, W., Huang, X. and Yao, J. (2019) NF-YC12 is a key multi-functional regulator of accumulation of seed storage substances in rice. *J. Exp. Bot.* **70**, 3765–3780.

Yang, J., Luo, D., Yang, B., Frommer, W.B. and Eom, J.S. (2018) SWEET11 and 15 as key players in seed filling in rice. *New Phytol.* **218**, 604–615.

Yokosho, K., Yamaji, N., Fujii-Kashino, M. and Ma, J.F. (2016) Functional analysis of a MATE gene OsFRDL2 revealed its involvement in Al-induced secretion of citrate, but a lower contribution to Al tolerance in rice. *Plant Cell Physiol.* **57**, 976–985.

Zee, S.Y. (1972) Vascular tissue and transfer cell distribution in the rice spikelet. *Aust. J. Biol. Sci.* **25**, 411–414.

Zhang, C. and Turgeon, R. (2018) Mechanisms of phloem loading. *Curr. Opin. Plant Biol.* **43**, 71–75.

Zhang, W.H., Zhou, Y., Dibley, K.E., Tyerman, S.D., Furbank, R.T. and Patrick, J.W. (2007) Review: nutrient loading of developing seeds. *Funct. Plant Biol.* **34**, 314–331.

Zhao, C., Xu, W., Song, X., Dai, W., Dai, L., Zhang, Z. and Qiang, S. (2018) Early flowering and rapid grain filling determine early maturity and escape from harvesting in weedy rice. *Pest Manag. Sci.* **74**, 465–476.

Zhou, S., Zhu, S., Cui, S., Hou, H., Wu, H., Hao, B., Cai, L. *et al*. (2021) Transcriptional and post-transcriptional regulation of heading date in rice. *New Phytol.* **230**, 943–956.

Supporting information

Additional supporting information may be found online in the Supporting Information section at the end of the article.

Figure S1 Comparison of major agronomic traits of wild-type (WT) and *gfd1* mutant.

Figure S2 Comparison of major agronomic traits of NIL^{ZH11} and *gfd1*-C1.

Figure S3 CRISPR/Cas9 knockout of *GFD1* in ZH11 and Nipponbare background.

Figure S4 Phenotypes characterization of ZH11 and KO1.

Figure S5 Phenotypes characterization of ZH11 and KO2.

Figure S6 Comparison of major agronomic traits of ZH11, KO1 and KO2.

Figure S7 Phenotypes characterization of Nipponbare and KO3.

Figure S8 Comparison of major agronomic traits of Nipponbare and KO3.

Figure S9 GFD1-GFP was agroinoculated into *Nicotiana benthamiana* leaves together with the Golgi marker Man49-mRFP or ERD2-mRFP.

Figure S10 Y_2H screening the interaction proteins of GFD1.

Figure S11 Y_2H screening the interaction proteins of GFD1.

Figure S12 CRISPR/Cas9 knockout of *OsSUT2* and *OsSWEET4*.

Table S1 Primers used in this study.

